Mine Closure 2026 – AB Fourie, G Boggs, J Heyes & M Tibbett (eds)

doi:10.36487/ACG_repo/2615_59

Quantifying rock stockpile infiltration for effective cover design: novel approaches to water management at the former Pitch uranium mine

Michael Hay [a,*], Guosheng Zhan [b], David Wykoff [b], Edward Lundvall [a], David Silverman [a], Tracie Jackson [b], Oscar Osores [b], Allison Brown [b]

[a] *Arcadis, USA*

[b] *Barrick Gold North America, Inc, USA*

Abstract

Designing effective water management strategies for mine reclamation is critical to meeting long-term closure objectives associated with geotechnical stability, surface reclamation and water quality. The infiltration rate into mine facility surfaces (waste rock stockpiles, heap leach pads, tailing impoundments) is a key parameter influencing the long-term water balance, which in turn influences constituent release and water quality. Mine facility infiltration is complicated by many factors such as particle size, material placement methods, and temporal factors such as long-term compaction. Having a detailed understanding of infiltration rates and how they vary across different portions of each mine facility can result in substantial optimisation of cap/cover approaches.

This study will describe an optimised cover evaluation approach currently underway at the former Pitch uranium mine. Waste rock stockpile seepage from infiltrating meteoric water is primarily associated with melting of snow that drifts by wind and accumulates on flat benches and within stormwater ditches rather than steep slopes. Data collection at the site has included a combination of lidar snow/bare-ground surveys, standard single-ring infiltrometers, in situ moisture sensors, and larger-scale ditch infiltration tests involving water addition and downstream flow measurement. Ditch flow infiltration test data have been evaluated using simple gain/loss water balance approaches, as well as a novel application of the Philip and Green-Ampt infiltration models. Spatial variability in surface hydraulic conductivity is quantified by running single-ring tests at different locations/slope angles and ditch tests of varying lengths; these results demonstrate lower permeability in ponding areas due to silt accumulation. This detailed analysis will be used in future evaluations of alternative cover options to limit infiltration for seepage reduction and to assess whether selective lining (bench/ditch impermeable lining with slope revegetation/reforestation) could be a more environmentally sustainable and cost-effective means of reducing infiltration.

Keywords: *uranium, water management, waste rock, infiltration, cover design, infiltration model*

1 Introduction

The Pitch mine is a former uranium mine near the Continental Divide in Colorado, USA. The site is located in a remote, alpine terrain at an elevation of more than 3,000 m above mean sea level and receives snow 7 months out of the year. Underground mining was conducted at the site from 1959 through 1962. In the 1970s, the mine site was acquired by Homestake Mining Company (HMC), and uranium was extracted via open pit mining from 1979 through 1984. Since that time, the site has been in care and maintenance, with substantial efforts to close the site ongoing from the mid-1990s through the present. Major features at the mine site include an open pit, saturated underground workings, and 2 rock stockpiles that received waste

* Corresponding author. Email address: michael.hay@arcadis.com

rock from underground and open pit mining: the approximately 50 ha Indian rock stockpile and the approximately 12 ha Tie Camp rock stockpile (Figure 1).

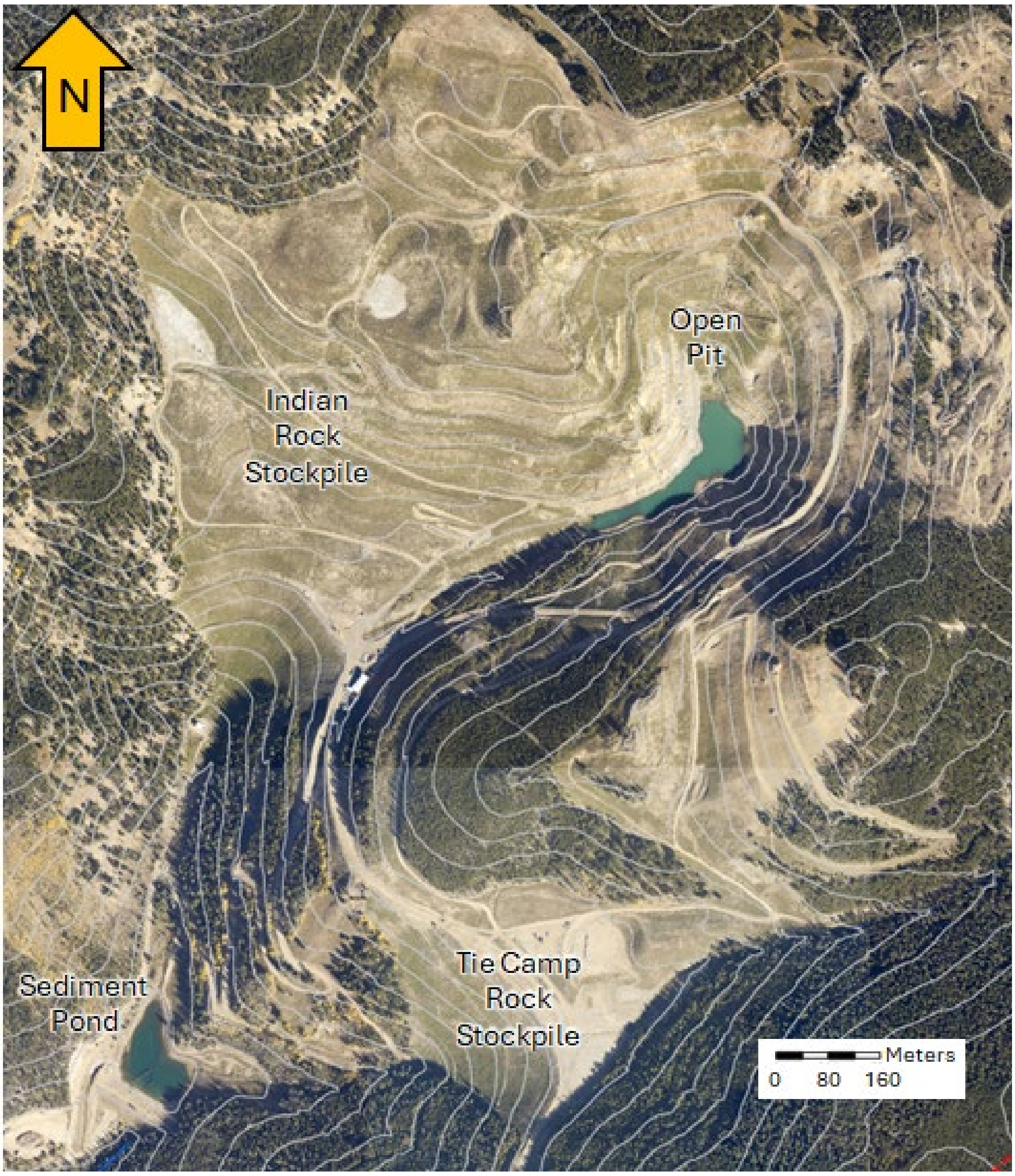

Figure 1 Pitch mine site features and 15-m interval topographic map

Recently, HMC has been evaluating approaches for reducing rock stockpile infiltration and their potential effectiveness. Any approach considered, such as capping and cover options, must weigh the potential reduction in water infiltration relative to the feasibility of implementing the remedy on steep slopes (which approach 3 [H] to 1 [V] or steeper on the waste rock stockpiles) and the overall effect on revegetation. In the 30-plus years since the waste rock stockpiles were established and contoured, substantial revegetation (including limited reforestation, which is anticipated over the long term) has occurred, and widespread cap/cover implementation could significantly set back reclamation efforts and limit future reforestation potential. Any system for minimising infiltration must also account for the fact that water flow at the site is primarily driven by snowmelt, with 50–90% of the precipitation at the site falling as snow within a given year.

The remainder of this paper presents the methods and preliminary results of a study implemented at the site to evaluate snow accumulation and infiltration on the rock stockpiles, with the objective of evaluating potential methods for minimising percolation.

The following components of the study are described in more detail:

- snow surveys to evaluate the extent and spatial distribution of snow deposition across the site, completed in 2023, 2024 and 2025, with a lidar snow survey conducted in 2023
- standard infiltration measurements, including single-ring infiltrometers, completed in 2024 and 2025
- a novel, non-standard infiltration measurement approach to evaluate water loss and infiltration in stormwater ditches, completed in 2025
- correlation of 2025 geotechnical measurements with onsite infiltration measurements.

The procedures implemented at this site are broadly applicable and could be implemented at other mine sites to optimise cap/cover and surface reclamation designs.

2 Snowpack extent and spatial distribution

Between 2023 and 2025, snow surveys at the site have been conducted to quantify snow thickness and snow density at peak snowpack, which typically occurs in early April each year. The snow survey includes snow probe and snow tube measurements at approximately 15–20 locations across the site. These snow tube surveys are completed each year to evaluate annual variability in snowpack and snow water equivalent.

In 2023, the snow tube survey was expanded to include a lidar survey of the snow surface at peak snowpack. The lidar survey was conducted by aeroplane on 31 March 2023, while peak snowpack at the site (as measured at the Porphyry Creek SNOTEL (snowpack telemetry) station approximately 9 km north of the site) occurred on 1 April 2023. By subtracting the snow surface elevation map from a similar bare-ground lidar map collected in October 2022, the snow thickness at peak 2023 snowpack across the site was estimated (Figure 2).

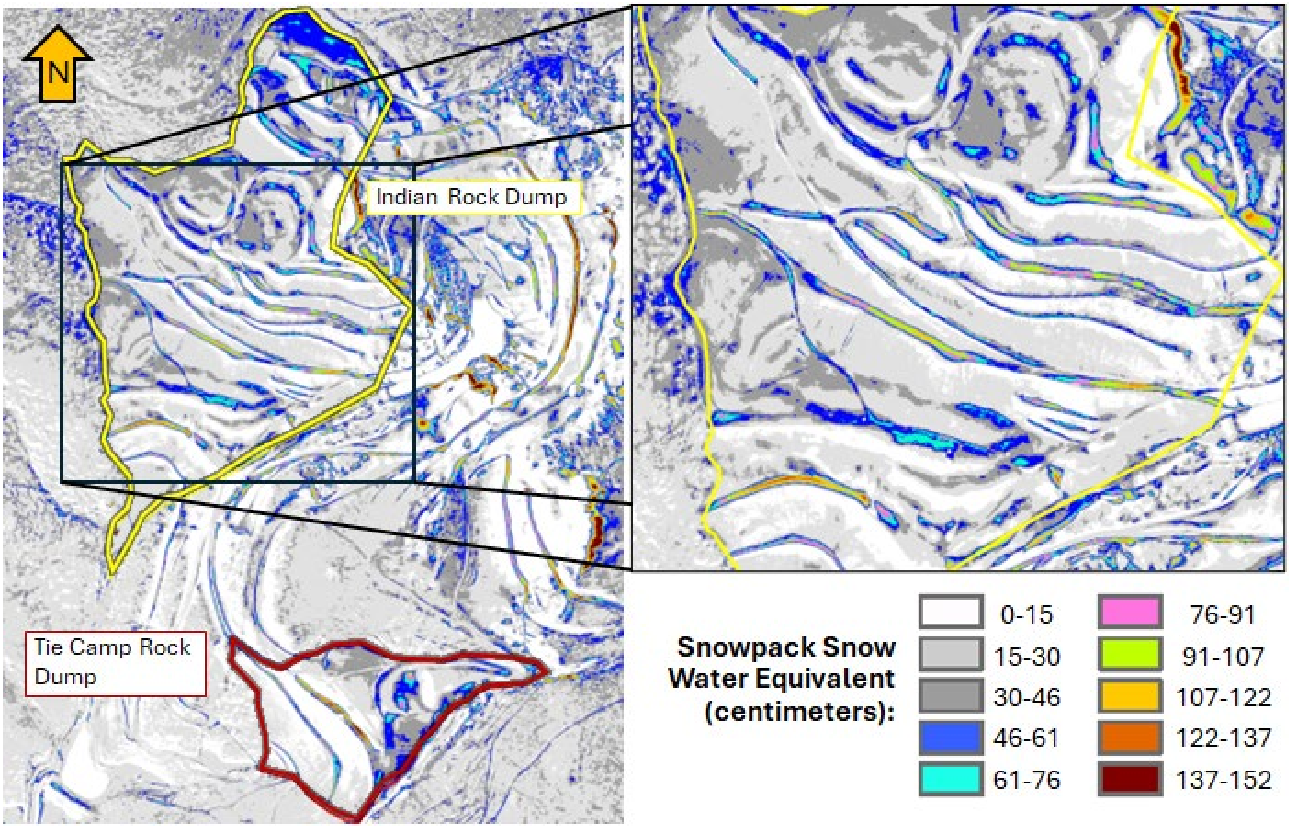

Figure 2 April 2023 snow thickness map, obtained by subtracting snow-covered and bare-ground lidar image maps

Key conclusions of the annual snow tube surveys and the 2023 lidar survey include the following:

- Snow thickness as measured by the snow tubes varied from less than 40 cm to over 190 cm on the Indian and Tie Camp rock stockpiles. Snow tube measurements indicated a snow density of 16–42%, with greater snow density corresponding to areas with greater snow depth (Figure 3a).
- Lidar imagery confirmed the range in snow depths across the rock stockpiles and demonstrated the preferential accumulation of snow along benches, drainage ditches and low-slope areas at the top of each stockpile. In contrast, steeply sloped areas had relatively less accumulation due to wind drifting (Figure 2).

The results of the snow survey highlight the importance of wind on the scouring of snow off slopes, leading to greater snow deposition in benches and drainage ditches. The up-valley (northeastern) direction of wind results in snow moving upslope, with greater accumulation on the tops of the stockpiles.

Because of the non-uniform snow deposition, a majority of the snow volume (and associated water volume) is associated with a relatively small area of the rock stockpile. Figure 3b plots the cumulative area covered and cumulative snow water volume (as per cent of total) as a function of the snow thickness 'cut-off' (expressed in snow water equivalent) – i.e. fraction of the covered area and water volume for snow thickness above a given value. For example, this plot illustrates that approximately 50% of the total snow water volume on the Indian rock stockpile was associated with snow pack greater than 37 cm, but this corresponded to approximately 27% of the rock stockpile area. As illustrated in Figure 2, these areas correspond to benches and drainages, not steep-sloped areas.

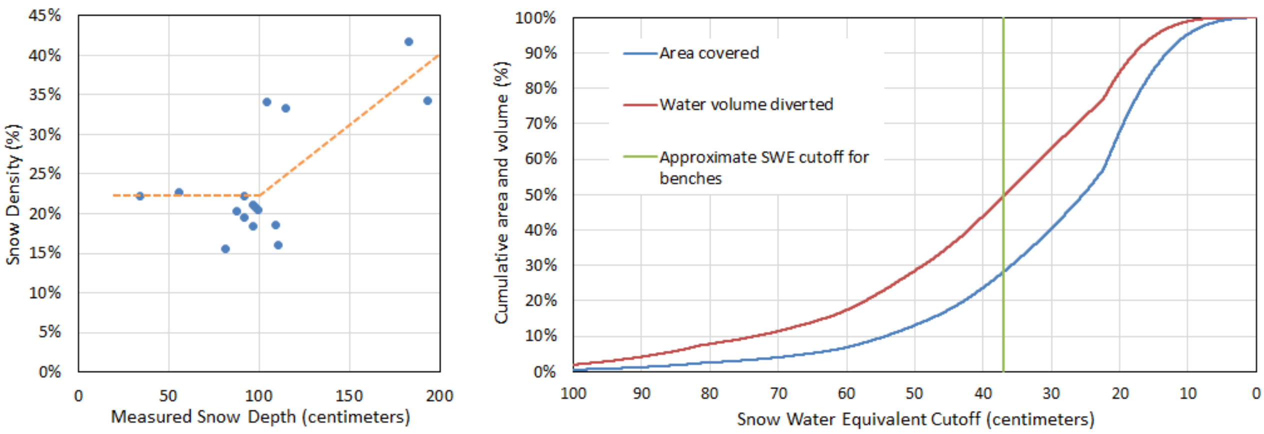

(a) (b)

Figure 3 Indian rock stockpile snow survey results. (a) Snow density versus measured snow depth; (b) Cumulative snow-covered area and snow water volume as a function of decreasing snow depth

3 Surface infiltration rates and field hydraulic conductivity

Infiltration testing was conducted to quantify surface hydraulic conductivity across the rock stockpile surfaces, including spatial and topographic variability. This parameter is important in evaluating the potential effectiveness and need for infiltration management, particularly to the extent that high slope/low conductivity surfaces may already be substantially limiting infiltration. Infiltration testing included geotechnical measurement on field samples, single-ring infiltrometers, ditch infiltration tests and installation of in situ soil moisture sensors. For method development, testing to date has focused on the Indian rock stockpile, but additional tests will be carried out at other portions of the site in the future. The sampling locations for each of the different analyses are shown in Figure 4.

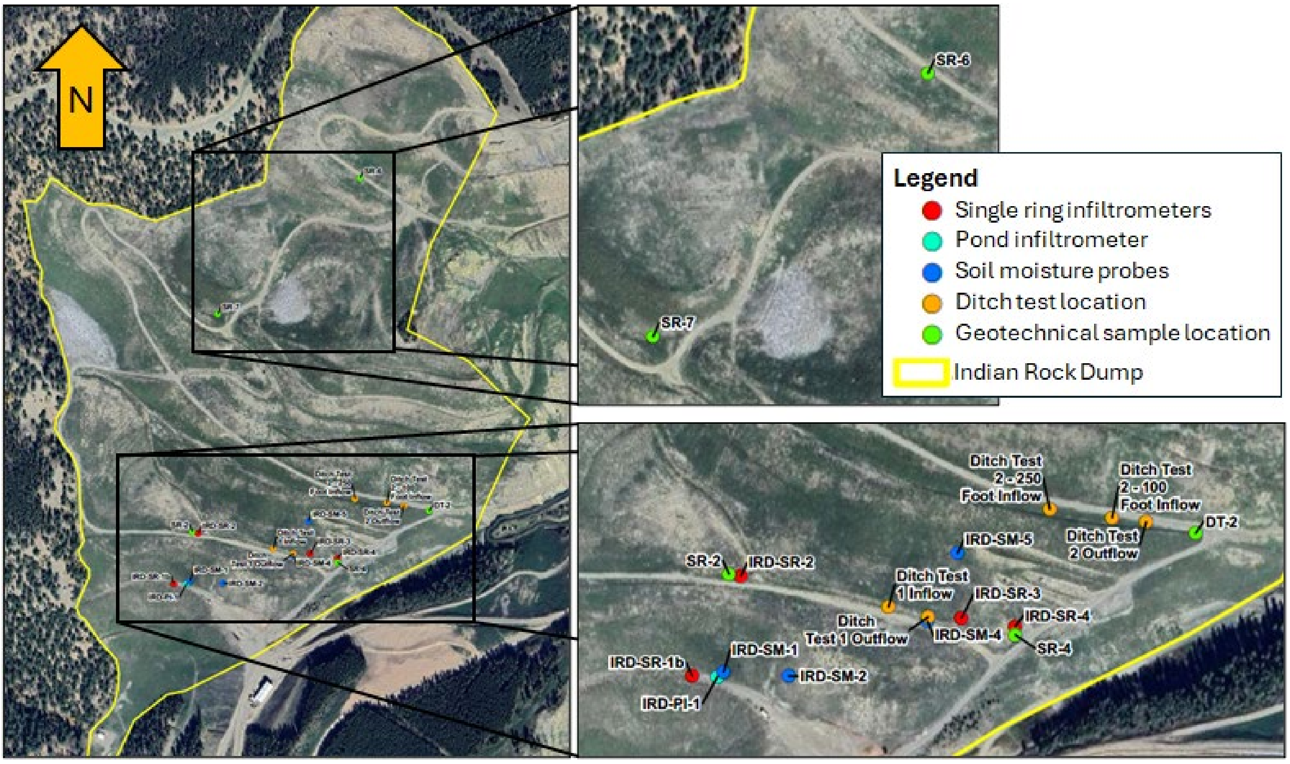

Figure 4 Infiltration test and sample collection locations

3.1 Geotechnical testing

Geotechnical testing included laboratory measurement of particle size distribution, gravimetric moisture content and hydraulic conductivity on samples collected from the surface of the Indian rock stockpile. Samples were collected from small test pits approximately 60 × 60 cm by 15–25 cm deep. Samples were collected from varying environments, including from within a stormwater ditch (DT-2), on gentle slopes adjacent to benches (SR-2 and SR-6), and within flat areas that receive ponding stormwater during rain events (SR-4 and SR-7). Samples were screened to less than 7.6 cm prior to shipping to the laboratory.

Particle size analysis results are provided in Figure 5. The results demonstrate that grain size is spatially variable across the Indian rock stockpile and generally poorly sorted, consistent with what is expected for waste rock material. Out of the 5 samples collected, the sample collected from within the drainage ditch exhibited the coarsest grain size distribution, whereas the 2 samples collected from flat ponding areas exhibited the greatest proportion of fine material (below #40 mesh). This is consistent with the anticipated result that finer silt/sand material is being washed from surface materials in the drainages and accumulating in flat areas that collect and retain water.

Based on the observed particle size distribution, 2 samples were chosen for hydraulic conductivity testing: the sample with the coarsest size distribution (DT-2) and sample with the finest size distribution (SR-4). Due to the finer-grained nature of sample SR-4, method ASTM D5084 (flexible wall permeameter; ASTM 2024a) was used, while method ASTM D5856 P (rigid-wall permeameter; ASTM 2024b) was used for sample DT-2. To approximate in situ conditions, the DT-2 sample was compacted with the goal of achieving a similar density as in situ conditions; the actual dry density of the test was 1.66 kg/L, which is similar to but lower than the in situ conditions (2.02 kg/L). It was expected that the compacted density in the laboratory would be less than the calculated in situ density because the in situ density included particles greater than 3 inches in diameter, which were screened out and not included in the material sent to the laboratory. Regardless, this lower density may have resulted in a slightly higher laboratory *K* values than in situ values in the field. The resulting hydraulic conductivities from the permeameter tests were 8.23×10^{-3} cm/s for DT-2 (geometric mean of 3 tests) and 3.0×10^{-5} cm/s for SR-4, demonstrating that material with coarser grain size and fewer fines (DT-2) exhibits a substantially higher hydraulic conductivity than the finer grain size material (SR-4).

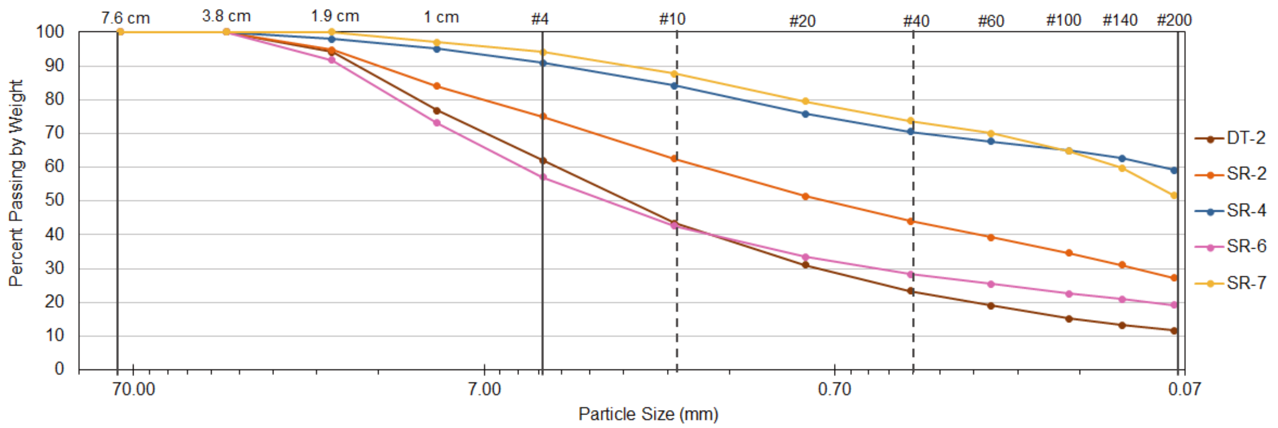

Figure 5 Particle size distribution results

3.2 Single-ring infiltrometers

In addition to the laboratory-based measurements, in situ field-based measurements of infiltration rate and hydraulic conductivity were also estimated. Infiltrometer testing was completed according to the Bouwer et al. (1999) method using 2 different ring sizes. The smaller single-ring infiltrometers were constructed from plastic 205 L drums and were 57 cm in diameter and 42 cm tall. A larger 'pond infiltrometer' was constructed from a plastic water tank, measuring 2.2 m in diameter and cut to 48 cm tall. Infiltrometers were set into the ground by a combination of digging around the edges and sealing the edges with hydrated bentonite; this latter step was particularly necessary in hard surfaces with coarse rock not amenable to shallow digging without substantial ground disturbance. Example photographs of the small single-ring infiltrometer and the pond infiltrometer are provided in Figure 6.

(a) (b)

Figure 6 Single-ring infiltrometers. (a) Small 205 L drum-scale ring; (b) Larger-scale pond infiltrometer

Tests were completed by adding water to the infiltrometers to a known height and then measuring the water level as water infiltrated over time. Additional water was added periodically to the infiltrometers, and the measurements were repeated. Because the rate of infiltration was relatively low (compared to the agricultural soils for which the test was designed), some tests spanned beyond a single day, and pressure transducers were deployed in each infiltrometer to track infiltration. Although these tests were left uncovered, the evaporation rate (estimated at up to approximately 1 cm/day during the summer at the site) is small compared to the infiltration rate, with evaporation accounting for less than 10% of the observed water drop in the infiltrometers.

An attempt was made to process the infiltration rate data using the Bouwer et al. (1999) method to estimate hydraulic conductivity; however, this processing method required results that were challenging to collect accurately in the field, including vertical and lateral wetting fronts at the end of the tests. Due to these data limitations, alternative methods for estimating the hydraulic conductivity using the models of Philip (1957) and Green & Ampt (1911) were used, as summarised by Sharief et al. (2023). Specifically, the Philip infiltration model expresses the infiltration capacity, f (L/T), as follows:

$$f = \frac{s}{2\sqrt{t}} + K \tag{1}$$

where:

s ($L/T^{1/2}$) = soil suction potential function or 'sorptivity'

t (T) = time after start of infiltration

K (L/T) = Darcy's hydraulic conductivity.

Note that in Equation 1 and in equations provided below, the units of each parameter are defined as follows:

L = length, in metres or centimetres depending on the parameter

L^3 = volume, typically in litres

T = time, typically in minutes or seconds depending on the parameter.

Without requiring determination of each of these terms, K can be estimated as the y-axis intercept of a fitted straight-line curve to a dataset of f versus $1/\sqrt{t}$. Individual values of $f(t)$ are estimated as the quantity of water infiltrated (i.e. the change in water level within the infiltrometer) between 2 measured time points.

Similarly, the Green-Ampt model also includes an expression for f from which K can be determined as the y-axis intercept of a straight-line curve. The Green-Ampt model expresses f (L/T) in terms of the effective soil porosity, η (unitless); the capillary suction at the wetting front, S (L); the hydraulic conductivity, K (L/T); and the cumulative infiltration depth, $F(t)$ (L) (calculated here as the total change in infiltrometer water level up to time t, correcting for infiltrometer refills):

$$f = \frac{\eta S K}{F} + K \tag{2}$$

Examples of the Philip and Green-Ampt fits to ring infiltrometer data are shown for sample IRD-SR-1B in Figure 7.

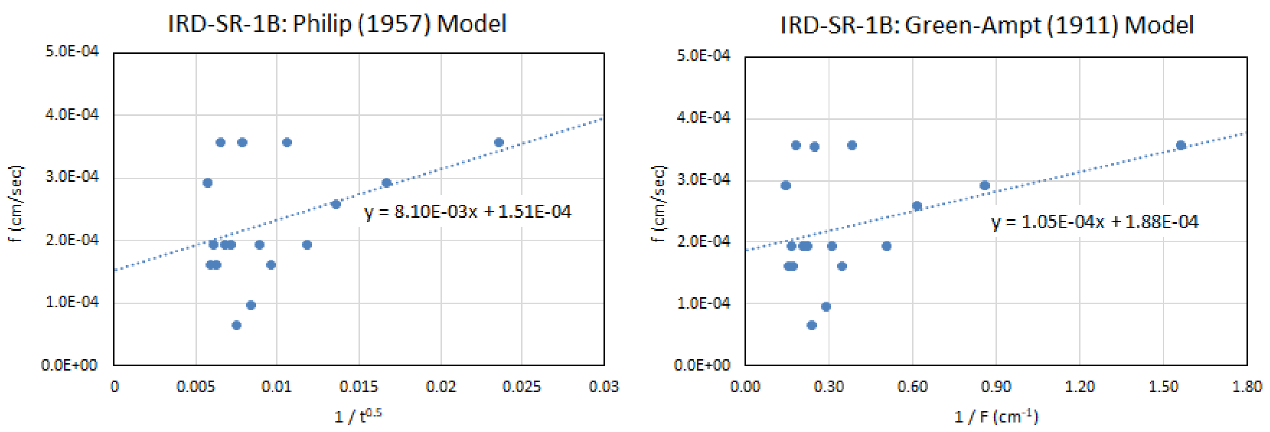

(a) (b)

Figure 7 Hydraulic conductivity estimation for IRD-SR-1B using a) Philip model (Equation 1); b) Green-Ampt model (Equation 2)

Results of the infiltrometer testing are summarised in Table 1. The hydraulic conductivities represent the geometric mean of the values estimated using the Philip and Green-Ampt methods described above, except for the IRD-SR-1A test, which only yielded a single infiltration rate value (in this case, the hydraulic conductivity was assigned as the infiltration rate).

Key observations include the following:

- The hydraulic conductivity estimates range between approximately 5×10^{-5} and 1×10^{-3} cm/s, which is consistent with typical values for silt to silty sand (e.g. Freeze & Cherry 1979).
- Results for the pond infiltrometer (IRD-PI-1; 8.2×10^{-5} cm/s) were very similar to but slightly lower than the results obtained using the smaller ring infiltrometer in a similar location (IRD-SR-1A/B; 1.5×10^{-4} to 1.7×10^{-4} cm/s), possibly indicating minor effects of test scale.
- The result obtained for IRD-SR-4 of 7.8×10^{-5} cm/s was similar to but slightly greater than the laboratory value of 3.0×10^{-5} cm/s (Section 3.1), demonstrating the utility of the laboratory-based measurement.

Table 1 Single-ring infiltrometer hydraulic conductivity results

Sample location	Test type	Philip model (cm/s)	Green-Ampt model (cm/s)	Geometric mean (cm/s)
IRD-SR-1A	Small ring	–	–	1.5×10^{-4}
IRD-SR-1B	Small ring	1.52×10^{-4}	1.88×10^{-4}	1.7×10^{-4}
IRD-SR-2	Small ring	1.03×10^{-4}	1.37×10^{-4}	1.2×10^{-4}
IRD-SR-3	Small ring	1.08×10^{-3}	1.24×10^{-3}	1.2×10^{-3}
IRD-SR-4	Small ring	5.67×10^{-5}	1.08×10^{-4}	7.8×10^{-5}
IRD-PI-1	Pond infiltrometer	8.00×10^{-5}	8.33×10^{-5}	8.2×10^{-5}

3.3 Ditch infiltration tests

One concern with the use of small-ring infiltrometer and laboratory geotechnical tests for evaluating surface hydraulic conductivities is that these tests may not adequately capture effects that occur over large distances in a macro scale, including spatial heterogeneity in grain size distribution or pockets of relatively coarse material that may result in preferential flow. Such effects may be particularly important in drainage ditches which receive concentrated flows of rain run-off and snowmelt.

To quantify larger-scale infiltration on drainage ditches, a drainage ditch infiltration study was designed and conducted along 2 rip-rap stormwater ditches in separate benches on the Indian rock stockpile (Figure 4).

The general procedure for the ditch tests was as follows:

- For each test segment, a trapezoidal flume with a pressure transducer was installed at the downstream end to measure flow (outflow). The water outflow rate was measured through time based on water level in the flume (as recorded by the transducer).
- At the upstream end, water was pumped into the drainage at a known rate for approximately 1–2 hours twice (2 phases, with a break of 1–3 hours between phases) while flow was measured at the downstream end. Flow was controlled using a ball valve and recirculation line and verified using a calibrated in-line pipe flow meter/totaliser. Target inflow rates were generally 80–90 L/min. Over the short 1–3 hour test period, evaporation is considered negligible.
- Periodically throughout the tests, the width and depth of wetting in the ditch segment were measured at approximately 3 m intervals along the test segments. Wetted widths were observed to remain relatively stable by the time the wetting front encountered the trapezoidal flume at the outflow.
- Infiltration rates (in units of length per time) were estimated from the 'flow loss' (i.e. the steady-state water inflow rate minus the outflow rate, in units of volume per time) divided by the wetted area (length and wetted width) of the segment.
- Vertical hydraulic conductivities were estimated from the infiltration rates, dimensions of the wetted segment, and the average height of the water column within the segment during the test.

Three tests were conducted during the accessible field season in 2025. The first test was run along a 30 m (100 foot [ft]) segment of the 3,160 m (10,360 ft) elevation bench (lower/southern test in Figure 4). The second and third tests were conducted at the same location on a higher bench (approximately 3,170 m [10,400 ft] level; Figure 4); the first test was 30 m (100 ft) in length, and the second test was extended to 76 m (250 ft) by moving the water inflow point an additional 46 m upgradient. The tests were completed in completely dry drainages, following several days of dry (no rain) conditions.

Figure 8 provides the measured flow rates at the discharge point and weir and calculated infiltration (the differences of 2) for ditch test 1. Following start-up of the test, the wetting front took approximately 10–15 minutes to report to the outflow weir as the dry drainage segment filled with water. Additional saturation of the drainage sediment occurred over the next hour, with steady-state flow conditions occurring near the end of test phase 1 and through the duration of test phase 2. The calculated inflow rates for each of the 3 tests are provided in Table 2.

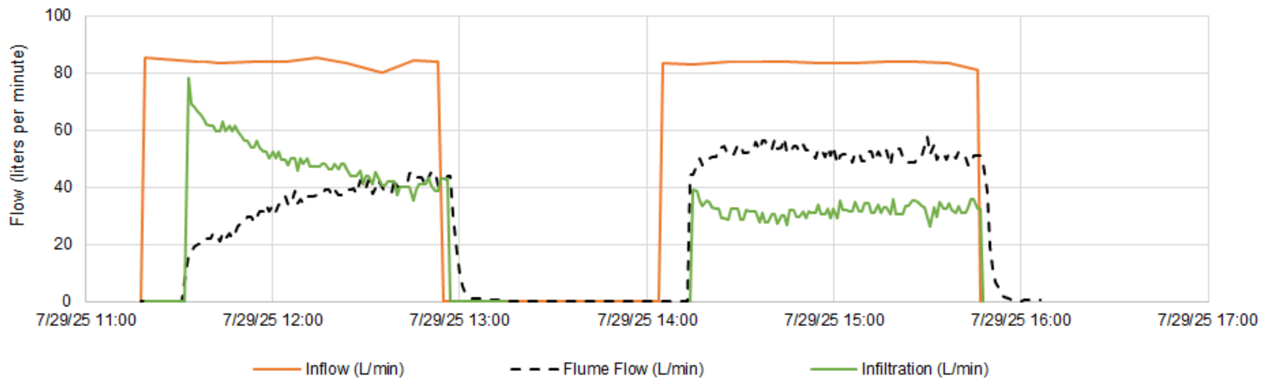

Figure 8 Ditch test 1 flow rate results

Table 2 Ditch test flow loss infiltration rates

Sample location	Steady-state inflow minus outflow (L/min)	Wetted area (m^2)	Infiltration rate (cm/s)
Ditch test 1	31.9	30.7	1.73×10^{-3}
Ditch test 2 – 30 m	18.3	15.4	1.98×10^{-3}
Ditch test 2 – 76 m	32.6	32.3	1.68×10^{-3}

The similarity in infiltration rates for the 30 m and 76 m ditch test 2 runs speak to the reproducibility of the results within a given section of drainage.

These data were then used to estimate surface hydraulic conductivity in 2 ways. In the first method, the infiltration rate was itself assumed to represent the effective hydraulic conductivity, with vertical and horizontal components distinguished to calculate vertical hydraulic conductivity from the steady-state flow dataset. The second approach used the Philip and Green-Ampt infiltration models described in Section 3.2. The methods and results are provided in the subsections below.

3.3.1 Vertical hydraulic conductivity estimation from steady-state infiltration rate

Vertical hydraulic conductivities, K_v, were calculated from the steady-state infiltration rates during the second phase of each test using the equations and assumptions below. This method assumes steady-state conditions and approximates the dimensions of the vertical and horizontal infiltration planes from observations of wetted width and estimates of the filled channel volume.

This method offers an approximation of hydraulic conductivity assuming the effective hydraulic conductivity, K_{eff}, is equal to the area-normalised infiltration rate during steady-state conditions:

$$K_{eff} = \frac{Q_{loss}}{L \times W} \tag{3}$$

where:

K_{eff} (L/T) = effective hydraulic conductivity

Q_{loss} (L^3/T) = calculated normalised infiltration rate

L (L) = wetted segment length

W (L) = average wetted segment width.

This equation follows from Darcy's Law, assuming a unit gradient.

The horizontal and vertical hydraulic conductivities are then estimated based on the average geometry of the wetted segment, where flow downward and out of the drainage is broken into horizontal and vertical components (see Figure 9 for a graphical illustration of variables):

$$K_{eff} = K_V\left(\frac{A_V}{A_{total}}\right) + K_H\left(\frac{A_H}{A_{total}}\right) = \frac{K_V LW + 2K_H LD}{LW + 2LD} \tag{4}$$

where:

K_V (L/T) = vertical hydraulic conductivity

K_H (L/T) = horizontal hydraulic conductivity

D (L) = average water depth

A_V = average saturated area along the bottom of the drainage ($L \times W$)

A_H = average saturated area along the sides of the drainage ($L \times D$)

A_{total} = total saturated area (sum of A_H and A_V).

Assuming K_H = 10 K_V and rearranging yields:

$$K_V = \frac{K_{eff}}{(LW + 20LD)/(LW + 2LD)} \tag{5}$$

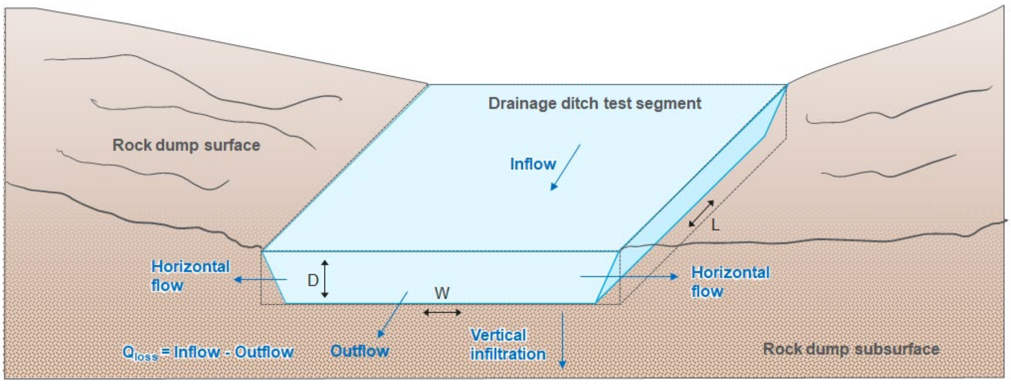

Figure 9 Schematic illustrating horizontal and vertical flow components out of drainage

An anisotropy ratio of 10 (K_H/K_V) is common in shallow unconsolidated material (e.g. Freeze & Cherry 1979); although this value can often be higher in alluvial deposits with clay minerals and highly layered geologic environments (up to 100 or more; Freeze & Cherry 1979), this would not be anticipated at the surface of a rock stockpile, where the anisotropy ratio may be less than 10. Note that as the anisotropy ratio approaches 1 (i.e. as K_H approaches K_V), the value of K_V approaches K_{eff}.

Estimated K_v results are provided in Section 3.3.3.

3.3.2 Philip and Green-Ampt hydraulic conductivity estimation

Hydraulic conductivities were also estimated using the Philip and Green-Ampt (Equation 2) functions described in Section 3.2. As with the single-ring infiltrometer data analyses, the hydraulic conductivity was estimated as the y-intercept of a straight-line fit to the infiltration capacity, *f*, as a function of $1/\sqrt{t}$ (for the Philip model; Equation 1) or 1/F (for the Green-Ampt model; Equation 2). The difference in this case is that, whereas the infiltration capacity in the infiltrometers was measured as a change in water level over a given time step, the infiltration capacity in the ditch infiltration tests was estimated based on segment flow loss, Q_{loss}. The Philip and Green-Ampt expression data fits are provided in Figure 10 for ditch test 1.

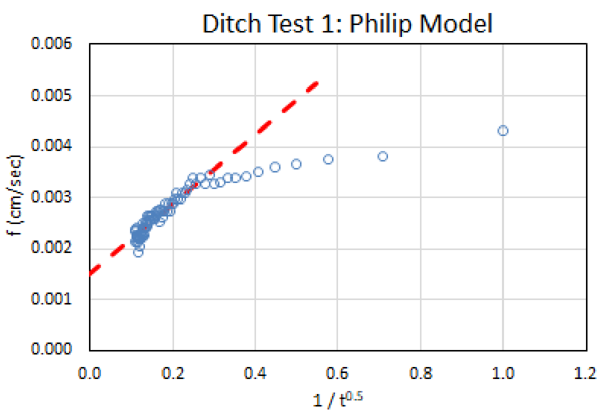

(a)

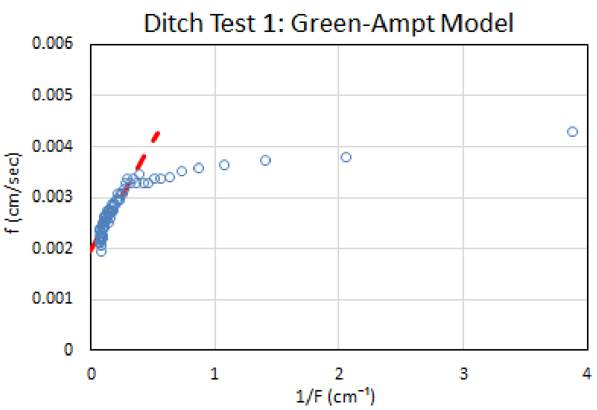

(b)

Figure 10 Hydraulic conductivity estimation for ditch test 1 using (a) Philip model (Equation 1); (b) Green-Ampt model (Equation 2)

The potential advantage of the Philip and Green-Ampt approach over the direct estimate of K_{eff} (or K_V as calculated in Section 3.3.1) is that the Philip and Green-Ampt functions do not necessarily require the infiltration to come to steady state before the hydraulic conductivity is estimated; it is expected that linearity in the Philip and Green-Ampt expressions may be observed before steady-state infiltration and segment outflow is observed. The results presented in Figure 10 are specifically for the Phase 1 results from ditch test 1 (period between 11:00 am and 1:00 pm on 29 July 2025 shown in Figure 8). The results in Figure 10 illustrate that linearity is not achieved in the ditch test results right away; in this case, the first 11 data points exhibit a shallower slope that would predict a higher intercept (higher hydraulic conductivity) than the later data points, likely due to artefacts (e.g. widening wetted segment width) at the very beginning of the test. However, the remainder of the data fit a straight line, starting after 11 minutes following reporting of water to the effluent flume (approximately 11:43 am). The Philip and Green-Ampt approach therefore provides a more robust, time-effective approach for quantifying hydraulic conductivity, while also providing an interpretation approach with fewer data restrictions.

3.3.3 *Stormwater ditch hydraulic conductivity results*

The results of the ditch infiltration hydraulic conductivity estimates are shown graphically in Figure 11.

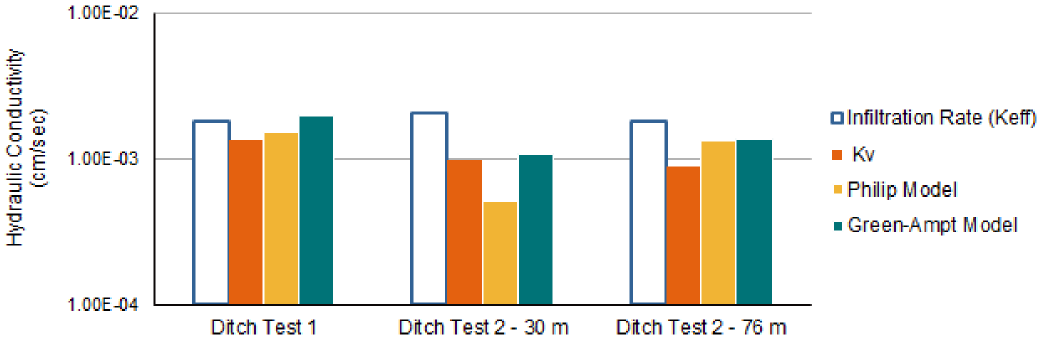

Figure 11 Comparison of ditch infiltration test infiltration rates and calculated hydraulic conductivities

As noted above, the difference between K_V and K_{eff} is dependent on the assumed anisotropy ratio, which was assumed to be 10. For an anisotropy ratio of 1 ($K_V = K_H$), $K_V = K_{eff}$.

These values may be further compared with the estimates from single-ring infiltrometers and laboratory hydraulic conductivity estimates.

Key observations are as follows:

- For the ditch infiltration tests, as anticipated, the Philip and Green-Ampt hydraulic conductivity estimates are typically lower than raw infiltration rates. In most cases, the Philip and Green-Ampt estimates are bracketed by K_{eff} and K_V estimated directly from infiltration. The Green-Ampt method estimates tend to be slightly higher than the Philip method estimates.
- Overall, the estimated hydraulic conductivities are between 5×10^{-4} and 2×10^{-3} cm/s. Although these tend to be higher than the ranges observed for the single-ring tests and the laboratory-measured values, the results are consistent with data collected close to the drainages. Specifically:
  - Geotechnical sample DT-2 was collected in the same drainage downstream of ditch test 2. The laboratory measured value of 8.24×10^{-3} cm/s was higher than the estimated range based on the ditch tests (between 5×10^{-4} and 1.4×10^{-3} cm/s) but was within an order of magnitude.
  - Single-ring infiltrometer test IRD-SR-3, although it was conducted outside of the drainage, was completed in close vicinity to ditch test 1 in an area receiving run-off. The estimated hydraulic conductivity at IRD-SR-3 (Philip and Green-Ampt geometric mean of 1.2×10^{-3} cm/s) was very similar to the results obtained for ditch test 1 (Philip and Green-Ampt geometric mean of 1.7×10^{-3} cm/s).

4 Surface infiltration dynamics

In addition to estimation of hydraulic conductivity, a preliminary attempt was made to evaluate infiltration dynamics using soil moisture sensors. Soil moisture sensors were installed at various depths within the rock stockpiles at 4 different locations (see Figure 4) to evaluate the rates and timing of the wetting front with infiltrating rain and snowmelt. IRD-SM-1 and 4 (located on flat benches, with IRD-SM-4 installed in a drainage ditch) had 4 sensors installed at 30 cm intervals down to 120 cm below ground surface, whereas IRD-SM-2 and IRD-SM-5 (placed on slopes) had 2 sensors installed at 30 and 60 cm below ground surface.

WaterScout SM100 soil moisture sensors (https://www.specmeters.com/) were installed by digging pits at the selected locations down to the target sensor depth, scraping the edge of the excavated pit to yield a vertical wall, and digging and emplacing each moisture sensor laterally into the wall of the excavated pit. The pits were then backfilled in lifts, with manual recompaction of the rock stockpile material as the pit was refilled to match pre-installation in situ density. The moisture sensors were connected with wires to a datalogger above the ground surface.

Soil moisture sensors were installed in summer 2024 and logged through summer 2025. The moisture probes were therefore in place during the winter 2024/2025 snowmelt and were also in place for various summer storm events in 2025. Example results are provided in Figure 12 for the moisture sensor array placed in the drainage ditch at IRD-SM-4, compared to the Porphyry Creek snowpack. Note that the soil moisture data were logged based on the default factory settings for moisture sensors and readers; as such, the soil volumetric water contents reported are not necessarily accurate on an absolute scale, but are instead used to evaluate relative changes as a function of time and between depths. For comparison in Figure 12, each of the 4 moisture sensors was normalised by the recorded value in March 2025. The plotted value is therefore the volumetric moisture content divided by the March 2025 measured moisture content.

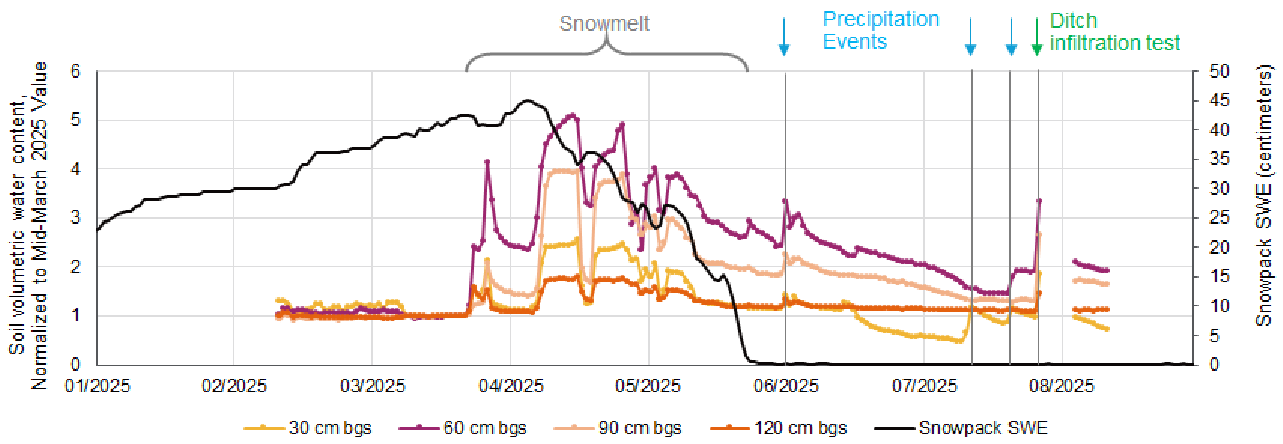

Figure 12 IRD-SM-4 soil moisture sensor results, 2024–2025

The soil moisture sensor results complemented the collection of snowpack and surface hydraulic conductivity estimations, providing key insights on water infiltration to depth under rain versus snow conditions.

Specifically:

- Soil moisture probes at all 4 depths responded to the gradual snowmelt that occurred from late March through early May, indicating percolation of snowmelt to depth.
- In contrast, several of the storm events yielded observable influence in shallow depths, with lesser influence in deeper zones. For example, the July storm events which resulted in resaturation at 30 and 60 cm depths were not observed in the 90 and 120 cm depths. This observation highlights the greater importance of temporary storage and evaporative release during short-duration summer rain events (limiting percolation to depth) compared to slow, extended snowmelt.

5 Conclusion

The combined evaluations of winter snowpack, infiltration evaluation and hydraulic conductivity estimation, and water infiltration dynamics provided key insights to inform potential future water management activities on the waste rock stockpiles at the former Pitch uranium mine.

The most important conclusions from this study are summarised as follows:

- Lidar and ground-based snow surveys demonstrated and quantified the extent of snow accumulation on benches and stormwater ditches, with limited accumulation on steep slopes. These quantitative results can be used to specifically quantify potential infiltration in different terrain to focus reclamation efforts.
- Measurement of infiltration with depth further confirms the importance of snowmelt relative to brief summer rain events in governing infiltration of water to depth, which appears to be a greater control on constituent release at this site.
- Hydraulic conductivity measurements demonstrate a high degree of spatial variability across the stockpile surface, but despite this spatial variability, logical differences were observed between run-off areas and lower permeability areas of water accumulation and ponding.

Overall, these results highlight the fact that sensible water infiltration management may not necessarily require a full impermeable cover over the full extent of the waste rock stockpile, particularly in the high altitude, forested, snow-driven environment applicable to the Pitch site. Instead, it is possible that more efficient and sustainable approaches could include selective lining of stormwater ditches and snow accumulation zones, coupled with recontouring, snow fencing, and/or strategic tree/vegetation planting to enhance snow collection in lined ditches and evapotranspiration on slopes. However, additional work will be needed to assess the long-term effectiveness and cost/benefit of selective lining. For example, under current conditions, snow scouring off slopes and snow deposition within benches is a key control on snow movement. Strategic reforestation would need to be implemented to ensure that the desired snow movement/deposition dynamics can be maintained.

Acknowledgement

The authors thank Homestake Mining Company for allowing site-specific information on the Pitch mine site to be published.

References

ASTM International 2024a, *Standard Test Methods for Measurement of Hydraulic Conductivity of Saturated Porous Materials Using A Flexible Wall Permeameter (D5084-24)*, West Conshohocken.

ASTM Standard , 2024b, *Standard Test Method for Measurement of Hydraulic Conductivity of Porous Material Using A Rigid-Wall, Compaction-Mold Permeame*ter (ASTM D5856-15), West Conshohocken.

Bouwer, H, Back, J & Oliver, J 1999, 'Predicting infiltration and ground-water mounds for artificial recharge', *Journal of Hydrologic Engineering,* October, pp. 350–357.

Freeze, R & Cherry, J 1979, *Groundwater*, Prentice Hall, Englewood Cliffs.

Green, W & Ampt G 1911, 'Studies on soil physics: I. Flow of air and water through soils', *Journal of Agricultural Science*, vol. 4, no. 1, pp. 1–24.

Philip, J 1957, 'The theory of infiltration: 4. Sorptivity and algebraic infiltration equations', *Soil Science,* vol. 84, no. 3, pp. 257–264.

Sharief, S, Zakwan, M & Farhana, S 2023, 'Estimation of infiltration rate using a nonlinear regression model', *Journal of Water Management Modeling*, vol. 31, pp. C509, https://doi.org/10.14796/JWMM.C509